11

Nano-Scale Reinforcing and Toughening Thermoplastics: Processing, Structure and Mechanical Properties

Suchart Siengchin
The Sirindhorn International Thai-German Graduate School of Engineering (TGGS), King Mongkut's University of Technology North Bangkok, Thailand

1. Introduction

Albeit the terms "nanocomposite" were introduced recently, such materials (e.g. carbon black filled rubbers) have been produced in industrial scale for more than five decades. Nowadays great effects are undertaken to improve the mechanical, thermal and other properties (e.g. flame resistance, barrier properties, electric conductivity) of polymers. To achieve this property upgrade nanocomposites are produced using fillers of various shape factors and dispersing them on nano-scale resulting in the formation of nanocomposites. The development of thermoplastics nanocomposites is rapidly emerging as a multidisciplinary research activity whose results could widen the applications of thermoplastics to the benefit of many different industries. Nanocomposites are a new class of composites that are particle-filled thermoplastics for which at least one dimension of the dispersed particle is in the nanometer range. In the related area thermoplastic/nanofiber composites have attracted considerable interest because they often exhibit remarkable property improvements when compared to virgin thermoplastic or conventional micro- and macro- composites. Accordingly, major goal of this book chapter is to explore a systematic study of enhancing the stiffness, strength and toughness characteristics of nanocomposites at the same time. In order to produce toughened nano-reinforced thermoplastics by water-assisted melt compounding, the toughener must be available also in aqueous dispersion. Moreover, most rubbers are available in latex form. Latex is a more or less stable aqueous dispersion of fine rubber particles being in submicron-micron range. The related particle size distribution strongly depends on the manufacturing of the latex. The mean size of the rubber particles in the latexes is exactly that what we need for toughening, impact modification of thermoplastics, in the range from 0.1-0.8 μm. The mean particle size is controlled by the viscosity ratio of the components and their interfacial tension in the melt.
In this book chapter different thermoplastic matrices are used (e.g. polyoxymethylene (POM) and polyamide-6 (PA-6)). Polyurethane (PU) and hydrogenated nitrile rubber (HNBR) were selected as the toughening agent for thermoplastics and used in its latex form. It is noteworthy that the mean size of rubber latices is closely matched with that of conventional toughening agents, impact modifiers. Synthetic nanofillers (e.g. carbon

nanofiber (CNF), boehmite alumina (BA) and sodium fluorohectorite (FH)) were used as reinforcements. One of the criteria for selecting these fillers was that they are water swellable/dispersible and thus their nanoscale dispersion can be achieved also in aqueous polymer latex.

2. Concepts of nano-scale reinforcement and toughness in thermoplastics

The major problem with nanoparticles reinforcement is that it causes severe material embitterment which is in close analogy with discontinuous fiber-reinforced thermoplastics. On the other hand, exactly this amount of nano –scale particles is needed to get optimum stiffness and strength properties. Blending the thermoplastic with elastomeric modifiers is a successful way to overcome this problem and to improve the toughness characteristics. Many works have documented the effect of various parameters of the modifiers on the toughness response including rubber particle size (Borggreve, 1987; Margolina & Wu, 1988), rubber concentration (Baldi et al., 2006) and interparticle distance (Wu, 1988; Jiang et al., 2002). These studies revealed that the rubber concentration should be above a critical level in function of its particle size. To improve the toughness of a polymer, the interparticle distance should fall below a critical value which depends on the volume fraction and the particle size of the rubbers. In this case, namely, the stress fields of neighboring particles overlap and a larger volume fraction of the matrix supports an average load higher than the applied load. Multiple localized plastic deformations are hereby initiated in the plastic zone ahead of the crack tip. Typical rubber particle sizes for effective toughening should be in nano-scale range. Rubber particles with micro size have been found to be relative inefficient, although they might be active in crack bridging.

In additional, the search for high performance nanofiber polymer composites produced successful results in related with toughness enhancements. Few research studies addressed the property improvements of polymers by adding carbon- nanofibers (CNFs) and nanotubes (CNTs). Most of CNF/CNT reinforced polymer composites show improvements in strength and stiffness with loss of elongation at break (Kumar et al., 2002; Chung, 2001; Sandler et al., 2002). There have been a number of experimental studies reported in the literature about the influence of CNT/CNF on the toughness enhancements of various types of polymers (Puglia et al., 2003; Song & Youn, 2005; Kinloch et al., 2002; Gryschuck et al., 2006). (Ruan et al., 2003) showed for enhancements in ductility of MWCNT/ reinforced ultrahigh molecular weight polyethylene (PE). The increased ductility in PE is most likely due to the chain mobility enhancement and attributed to the secondary crystal formation due to the presence of MWCNT. (Lozano et al., 2004) published extremely high extensibility; high toughness of CNF reinforced polyethylene bulk composites. The total tensile elongation of more than 1600% is higher than any published value for nanoreinforced composites. The large ductility increase in PE has been attributed to the excellent dispersion of CNF and interfacial bonding produced by the high shear history. In addition, CNF has been applied as the toughening filler of the structural material for resin based composites. (Seyhan et al., 2009) reported that the addition of low content of silanized vapor grown carbon nanofiber (VGCNF) improved the fracture toughness of the epoxy resin by about 12%. They concluded that attachment of epoxide end groups containing silane molecules to surfaces of CNF enhanced the compatibility between CNF and epoxy. Considerable interest is devoted to nanocomposites due to the attractive properties. It has been shown that the dielectric and mechanical properties of polymer based nanocomposites were markedly

improved by the addition of CNF (Sui et al., 2008, 2009). Similar to CNT, CNF has also a high reinforcing efficiency. Its presence in a small amount in the corresponding polymer, typically less than 5 wt. %, can result in significant improvement in mechanical properties. It has been reported that adequate interfacial adhesion of CNF to the related matrix and its uniform dispersion are the key factors in respect to the reinforcing effect (Prolongo et al., 2009). The length of CNF can very between 50 and 100 μm, therefore high aspect ratios can be obtained. As previously reported, CNF were purified and functionalized to remove amorphous carbon and to open the highly tangled fiber (Lozano et al., 1999). Being much longer than CNT, the disentanglement, dispersion of CNF is very problematic. The goal of improving the carbon nanofiber matrix interfacial adhesion issue and complete dispersion must be solved before achieving the full potential of CNF nanocomposites.

3. Preparation of nanocomposites

It was early noticed that the preparation technique of the nanocomposites has a strong impact on the dispersion of the nanoparticles (Park et al., 2007). Accordingly, various methods, like in-situ polymerization, melt blending and solution/dispersion techniques have been tried to disperse nanoparticles/nanofibers in polymers. In situ polymerization is a challenging one, as it allows us to adjust the chemistry to optimize the affinity between filler and the resulting polymer. Different types of polymerization methods have been used to prepare polymer nanocomposites, such as solution, suspension or emulsion, and free radical polymerizations (Akelah & Moet, 1996; Wang et al., 2002; Chen et al., 2000; Zhou et al., 2001). This variety to prepare polymer nanocomposites by in situ polymerization was mostly explored with clays. However, this process is cumbersome and also costly. If the organophilic modification of inorganic fillers could be eliminated, the procedure might be simplified and the production cost substantially lowered compared to state-of-art processes.

The use of conventional melt compounding techniques to prepare nanocomposites is usually more practical and economical than in situ polymerization. For that purpose common polymer processing equipments, such as extruders and internal mixers are suited. The shear, accommodated in the melt during processing may also be helpful to support the nanoparticles dispersion. However, it is not always enough to break up big particles agglomerates as the resulting nanoparticles dispersion may remain further poor. A homogeneous dispersion of nanoparticles in a polymer by using conventional compounding techniques is very difficult due to the strong tendency of fine particles to agglomerate (Jana & Jain, 2001). An alternative way to prepare composite materials is the latex compounding/latex coagulation technique. Latex compounding is a promising technique compared for example to in-situ polymerization and solution techniques which are used to produce nanocomposites. It is becoming more and more important because of the following benefits: simple many polymers are available in latex form, as typically Figures 1a-b shown in TEM image of PS latex (Siengchin et al., 2007) and AFM image of HNBR latex, respectively. The mean particle size is at ca. 200 nm and the particles are present in a very narrow distribution (cf. Figure1a). Latex can be introduced in polymer melt during compounding in line.

In an aqueous polymer latex, microscopic solid polymer particles are suspended in water. During drying they form a film through coalescence. When combined with nano-sized filler, the polymer particles and the filler create a segregated network. This may show excellent

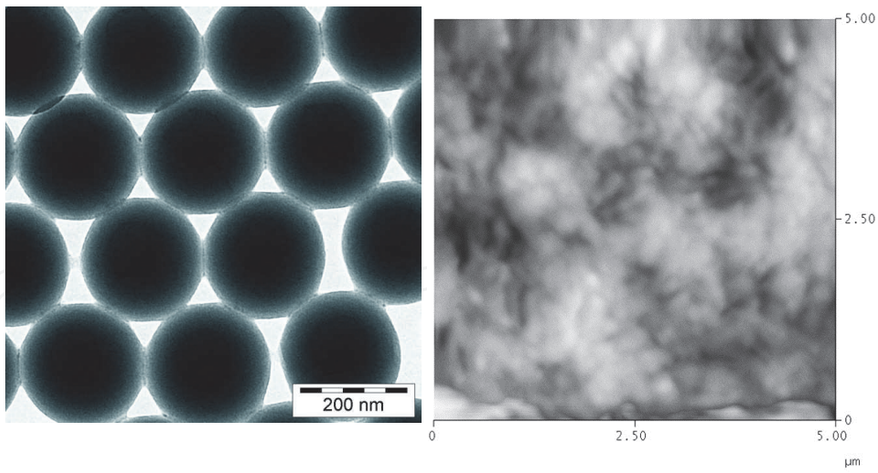

Fig. 1. (a) TEM image of PS latex (Siengchin et al., 2007) and (b) AFM image of HNBR latex.

properties at very low filler concentration (Grunlan et al., 2004), compared to a melt blended version containing the same polymer and filler. The advantage of this latex compounding process is that reduced health risk, good dispersibility, the expensive chemical modification of the fillers, giving the necessary affinity to the polymer, can be avoided. Moreover, when the nanofiller is well dispersed in the polymer latex, the latter can be used as a masterbatch (dry and liquid forms) for subsequent melt compounding. In addition, nanofiller containing latices or slurries can be injected in the melt during continuous melt compounding. Exactly, these are those options which have been explored in this chapter.

3.1 Latex melt compounding (LMC)

One very promising technique being developed for nanocomposite is latex melt compounding. Polymer blend, binary and ternary composite systems can be prepared by melt compounding using a masterbatch produced from polymer latex containing nanofillers (masterbatch technique, MB). A scheme of the masterbatch technique of polymer composite systems is given in Figure 2. First, an aqueous nanofillers slurry was produced at ambient temperature through mechanical stirring. Then the rubber latex was introduced in this slurry and stirred. The resulting slurry was poured in a framed glass plate and dried for few days at room temperature (RT). This resulted in a rubber film as the glass transition temperature (T_g) of rubber (PU or HNBR) is much lower than RT. The nanofiller-containing rubber masterbatch (MB) was introduced in the polymer system after melt mastication of the latter for few min. The overall duration of the melt mixing for blend, binary and ternary nanocomposites was prepared by laboratory kneader at the same condition.

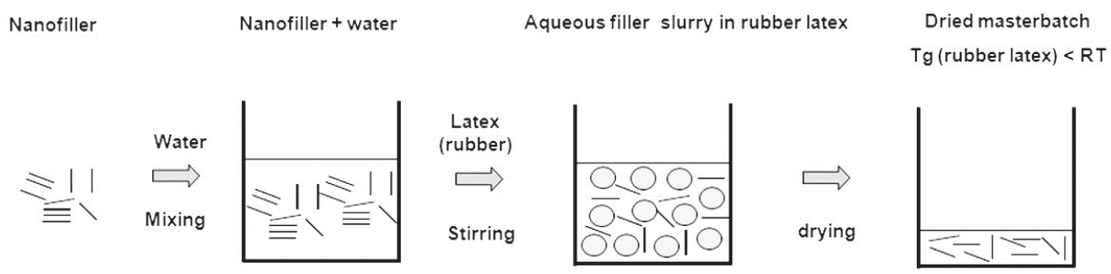

Fig. 2. Scheme of polymer nanocomposites prepared by the masterbatch technique.

3.2 Water-assisted melt compounding (WMC)

In this water-assisted melt compounding method, different nanoreinforced and/or toughened thermoplastics -based composite systems can be produced continuously in a twin-screw extruder whereby nanofillers in water slurry and rubber latices are introduced in the polymer melt. For compounding of the composites a conventional mixing screw was used the design of which is given in Figure 3. First, nanofillers were dispersed in water at ambient temperature under continuous mechanical stirring to obtain the aqueous nanofillers slurry. Thermoplastics–based composite systems were supplied so that sum totals were set to 10 kg/h. Rubber latex and/or aqueous nanofiller slurry were injected into the extruder, using pump. The extrusion temperature was selected between 150 °C and 190 °C systems from hopper to the die for all composite. Polymer pellets were charged in feeder in the first zone of the extruder. As shown in Figure 3, the nanoreinforced and/or toughened thermoplastics -based composite were prepared by using a pump: the resulting nanofiller slurry/rubber latex was injected in the melting zone into the extruder. A second pump was used to produce the ternary composite, whereby the rubber latex was introduced also in the barrels section 4. The water was eventually degassed in the transport zone (barrels section 7-9) of the screw and the evaporation was completed using a vacuum pump.

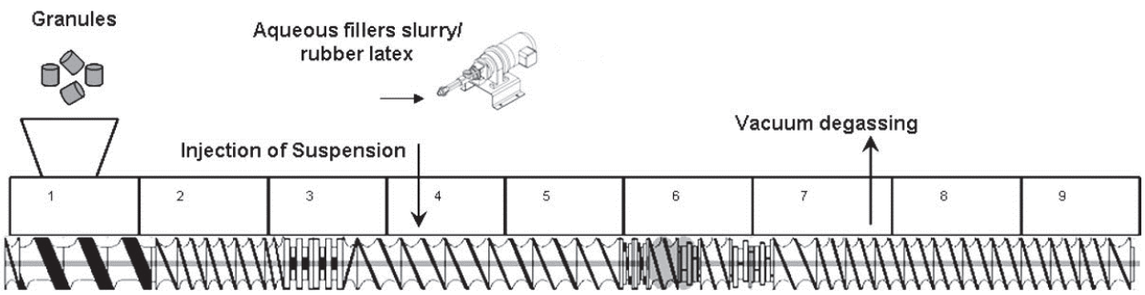

Fig. 3. Screw configuration and barrel sections of the co-rotating twin-screw extruder.

4. Structure – property relationships

From an effective process development point of view, it is interesting to be able to understand the relationships between process setting, physical molecular structure and (thermo) mechanical properties of nanoreinforcing and toughening thermoplastics. To obtain these relationships, a systematic study was performed on different characterization techniques for the related nanocomposites. The dispersion of nanofillers was characterized by transmission, scanning electron and atom force microcopies (TEM, SEM and AFM, respectively) techniques. The mechanical and thermomechanical properties of the composites were determined in Charpy impact, dynamic-mechanical thermal analysis (DMA), creep, stress relaxation tests, and thermogravimetric analysis (TGA). In additional, the dielectric response of nanocomposites was investigated by means of broadband dielectric spectroscopy.

4.1 Nanocomposites produced by LMC

4.1.1 Creep response

Nanocomposite materials used for structural applications of practical interest may exhibit viscoelastic behavior which has a profound influence on their performance. Viscoelasticity is

of interest in materials science and engineering since it is causally linked to a variety of microphysical processes and can be used as an experimental probe of those processes. The causal links between viscoelasticity and microstructure are explored in various viscoelastic tests. The viscoelastic behavior of polymers and related composites is usually characterized in creep test (whereby the creep strain is measured in time under a constant load) or dynamic mechanical test, where the variation in storage and loss moduli is observed as a function of the temperature, (Xia et al., 2007; Eckstein et al., 1998).

To describe the creep results, phenomenological models, composed of spring and dashpot elements, are frequently used. A spring element (elastic) behaves exactly like a metal spring, stretching instantly when stress is applied, maintaining the stress indefinitely, and returning to its original dimension instantly when stress is removed. In a dashpot (viscous) under stress, the plunger moves through the fluid at a rate that is proportional to the stress. In a creep experiment, the stress is kept constant and the change in the deformation of the polymer as function of time is recorded.

In the linear viscoelastic range, the parameters of this series do not depend on the level of the applied load. For creep under applied constant stress σ_0, the material response is:

$$D(t) = \frac{\varepsilon(t)}{\sigma_0} \tag{1}$$

where D(t) is the viscoelastic creep compliance and $\varepsilon(t)$ is creep strain at time, t.

In the nonlinear range the dependence upon the level of the applied load can be expressed by multiplying the linear parameters by so-called nonlinearity factors, which, of course, are load, time and temperature dependent (Schapery, 1969; Brueller, 1987). The nonlinear creep compliance is given by:

$$D(t,\sigma(t),T) = \frac{\varepsilon(t,\sigma(t),T)}{\sigma_0} \tag{2}$$

where $\sigma(t)$ is the real stress at time, t and T is temperature. This equation can be simplified with:

$$\varepsilon(t,\sigma(t),T) = \varepsilon(t,\sigma_0,T) = \varepsilon(t,T)c\sigma_0 \tag{3}$$

Thus, the following equation can be also expressed in terms of creep compliance

$$D(t,\sigma(t),T) = D(t,\sigma_0,T) = c\varepsilon(t,T) \tag{4}$$

where c is a constant. In the above equation creep compliance is only a function of the time and temperature.

Creep test is an important method to study the reinforcing ability of nanofiber in the thermoplastic matrix. As shown in Figure 4, the effects of CNF and PU incorporations on the creep response of POM (Siengchin et al., 2010). Introducing CNF into POM resulted in a considerable reduction in the creep as shown by the plots of creep compliance vs. time. Accordingly, CNF acts as reinforcing phase in POM. However, the presence of PU rubber particles increases the creep compliance data. SEM picture also confirms that the CNF is well dispersed in POM matrix (cf. Figure 5). Additional incorporation of CNF into the

POM/PU blend improves the resistance to creep confirming the reinforcing action of CNF also in this blend.

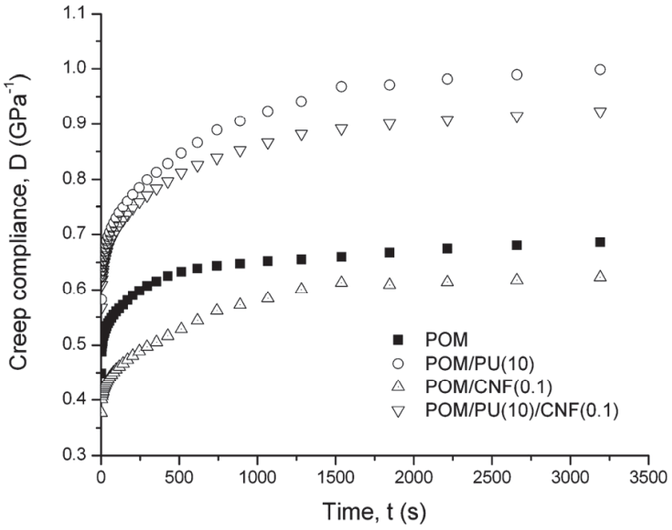

Fig. 4. Creep compliance for CNF based on POM composites (Siengchin et al., 2010).

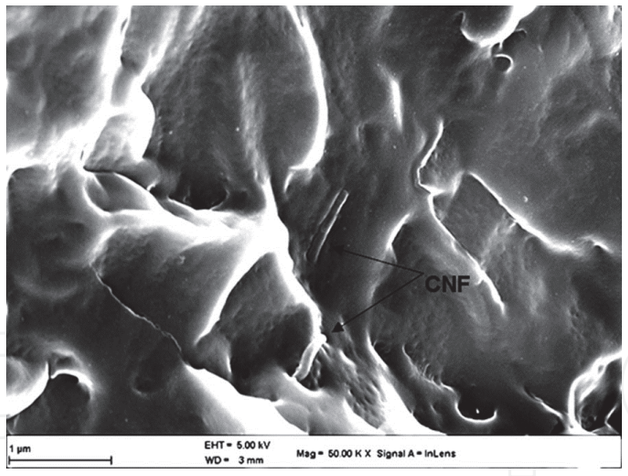

Fig. 5. SEM image of POM/CNF composite (Siengchin et al., 2010).

The considering outcomes are schematically depicted in Figure 6. The external mechanical loading included changes on lamellar level in a semicrystalline polymer, first lamellae rotation and separation take place after the amorphous molecules are highly stretched. These rotation and separation mechanisms, the occurrence of which depends on the relative orientation of the lamellae in respect to the loading, are at work also in the linear viscoelastic range. The nanofibers, being restricted by polymer chains and adhering well to the matrix strengthen the amorphous phase. So, the stretching of the amorphous and entangled chains occurs with considerable time delay under the same load in presence than in absence of

nanofiber. On the other hand, the rubber particles act as stress concentrators due to the high difference in the elastic modulus between thermoplastic and rubber. This stress concentration effect supports the stretching of the amorphous chains. The lamellae separation and rotation are also favored via the tie-molecules. The outcome is increased creep and creep rate.

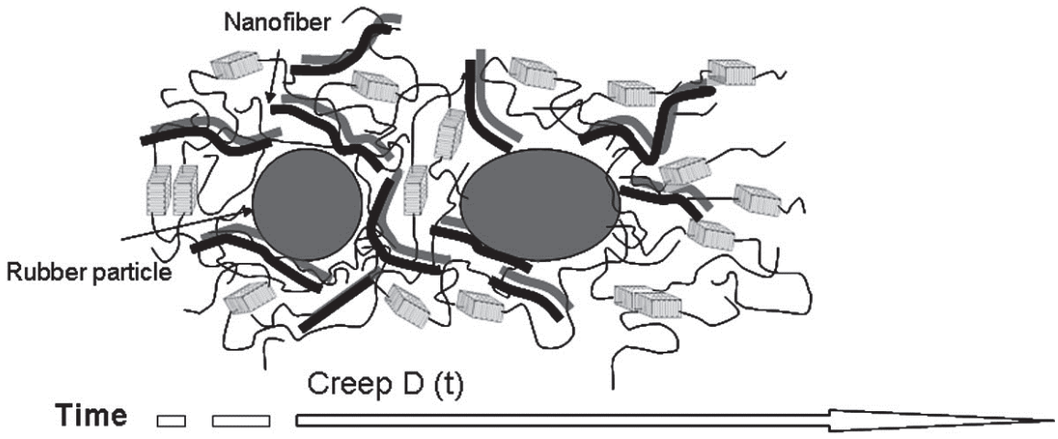

Fig. 6. Schema of creep development in reinforcing and toughening semicrystalline polymer.

(Siengchin & Karger-Kocsis, 2009) investigated by considering the morphological differences between the PA-6/HNBR/FH and PA-6/HNBR/BA and found that the FH stacks are dispersed in the PA-6 and located in the HNBR/PA-6 interphase. By contrast, BA is mostly embedded in the HNBR phase (cf. Figure 9). This creep effect is strongly suppressed in the FH-containing system due to the location of the FH in the interphase region. Embedding of BA in the HNBR reduced also the creep and creep rate as the stress concentration effect is diminished compared to the PA-6/HNBR binary blend. This reduction is due to the fact that the difference in the modulus between PA-6 and HNBR became smaller owing to the BA reinforcement of HNBR.

Further hints for the enhancement in the creep result were caused by the dispersed state (Siengchin et al., 2008). The authors found that the addition of PU into POM matrix resulted in a considerable increase in the creep compliance. The creep compliance values of the composites are smaller compared to the POM/PU blend showing the reinforcing effect of the alumina. The most striking finding is that the primary particle size of the alumina likely affects the creep behavior. More exactly the dispersion state of the alumina, are well reflected in the creep response. The change from micro- to nanocomposite reduces further the creep compliance. This may be associated with pronounced changes in the creep rate. A more interesting observation is that the creep response of all POM systems is sensitive to the temperature. This resulted in an increase in the mobility of the amorphous segments.

4.1.2 Dynamic mechanical thermal analysis

In addition of creep experiments, dynamic mechanical thermal analysis (DMA) is quite common method understand better some of the added complications that arise from the time and temperature dependence of the modulus of viscoelastic materials. Usually, the viscoelastic behaviour can be determined by measuring the storage modulus and the loss modulus over a wide range of frequencies and temperatures. The storage modulus is proportional to the

degree of elasticity of the system. The loss modulus is proportional to the dissipation or loss energy as heat in a cycle deformation, reflecting a certain degree of the viscosity of the system (Shaw & MacKnight, 2005). Figure 7 illustrates a schematic of dynamic experiment which shows graphically the nature of the two sinusoidal signals against time.

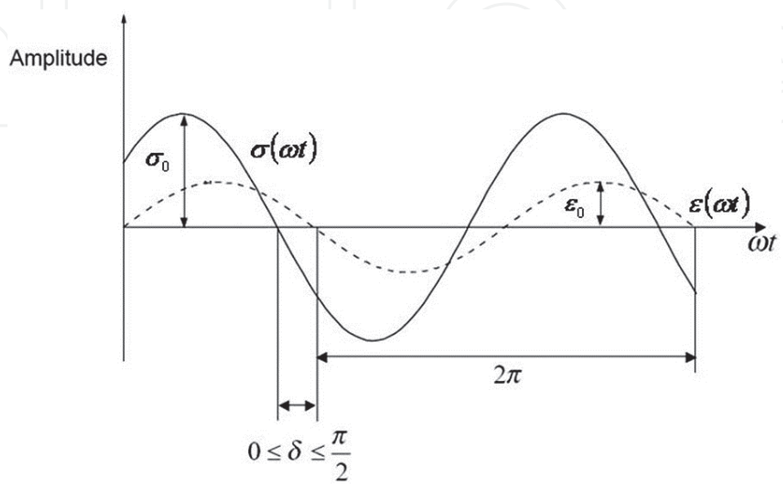

Fig. 7. Schematic of the dynamic mechanical experiment.

Consider the application of a sinusoidal strain, which can be presented by:

$$\varepsilon(t) = \varepsilon_0 \sin \omega t \tag{5}$$

where ε_0 is the maximum amplitude of the strain, ω is the angular frequency and t is time. The phase of the strain is arbitrarily set at zero, which can be done without loss of generality (perfectly elastic). The resulting stress $\sigma(t)$ is given by:

$$\sigma(t) = \sigma_0 \sin(\omega t + \delta) \tag{6}$$

A complex Young's modulus (E*) reflects the contribution of both storage (E′) and loss (E′′) components to the stiffness of material, as follows:

$$E^* = \frac{\sigma_0}{\varepsilon_0} = E' + iE'' \tag{7}$$

According to schematic of DMA, the modulus at these two points can be calculated from equations 6 and 7. The storage modulus (E′) gives directly:

$$E' = E^* \sin \delta \tag{8}$$

And in term of loss modulus (E′′):

$$E'' = E^* \sin(\pi / 2 + \delta) = E^* \cos \delta \tag{9}$$

The ratio of the loss modulus to the storage modulus is the tangent of the phase angle shift δ between the stress and strain vectors, thus:

$$\tan\delta = \frac{E''}{E'} = \frac{\sigma''}{\sigma'} \tag{10}$$

(Siengchin & Karger-Kocsis, 2009) examined the effect nanofillers, viz. FH and BA, in a HNBR toughened polyamide-6 in dynamic mechanical thermal analysis. DMA spectra in form of storage modulus (E′) and loss factor (tan δ) as function of temperature were plotted and are demonstrated in Figures 8, respectively. It can be seen in Figure 8a that the blend with 9 wt% of HNBR exhibits markedly lower stiffness than the PA-6 at least below the glass transition temperature (T_g) of PA-6 (ca. 50 °C). This is due to the rubbery character of the incorporated HNBR. However, the incorporation of sodium fluorohectorite (FH) and Boehmite alumina (BA) particles resulted in increase in the storage modulus in the whole temperature range, compared to that of the PA-6/HNBR blend. This can well be explained by the reinforcing effect of the nanoparticles leading to increased stiffness. One can also recognize that the storage modulus of FH is higher than BA nanocomposites. This stiffness increase suggests that FH stacks are well dispersed in the PA-6 matrix and have much higher aspect ratio in comparison with BA. This, along with the fact that BA was encapsulated in the HNBR phase, was confirmed by SEM image (cf. Figure 9).

The plots in Figure 8b reveal the T_g of PA-6 (at ca. 50 °C) and a strong secondary transition at ca. -50 °C. The latter peak in PA-6 (β-relaxation) is usually attributed to the mobility of non hydrogen bonded amide groups on adjacent chains (Araújo et al., 2004). Incorporation of HNBR yielded an additional maximum at -18 °C (T_g of HNBR) in the tan δ vs. T curves. Filling with BA and FH particles was accompanied with a shift in the T_g of PA-6 towards higher temperature (ca. 70 °C). The increment in the tan δ by adding HNBR is due to chain flexibilization, likely in the interphase regions. However, the tan δ values were reduced after additional incorporation of the nanofillers, as expected. The T_g of the HNBR may also be affected by the fillers. The related change may be traced to the preferred location of the corresponding fillers.

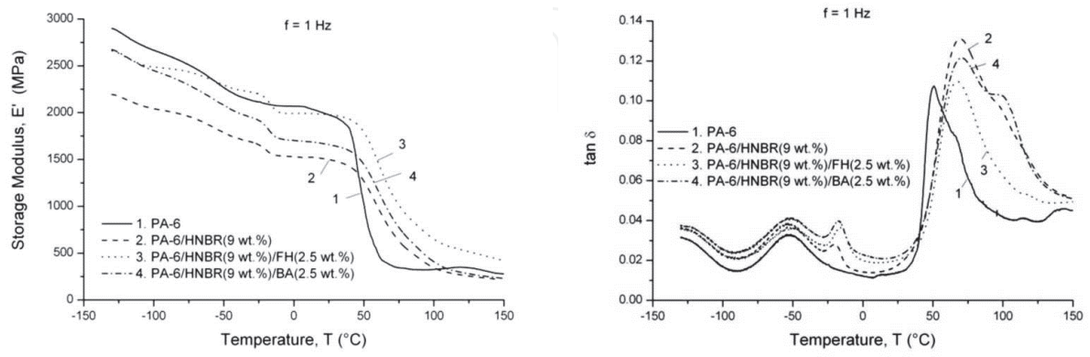

Fig. 8. (a) Storage modulus (E′) and (b) mechanical loss factor tan (δ) as a function of temperature for FH and BA based on PA-6 composites (Siengchin & Karger-Kocsis, 2009).

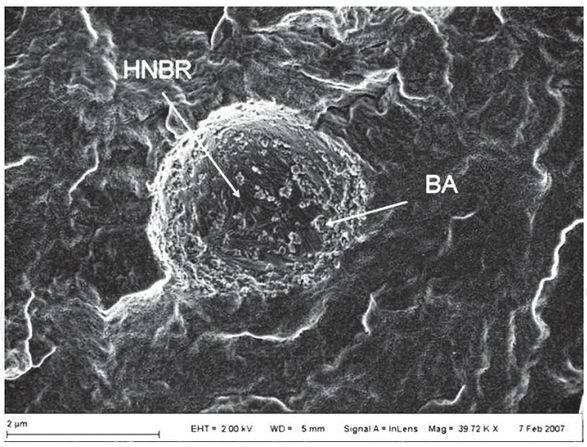

Fig. 9. SEM image of PA-6/HNBRBA ternary composite (Siengchin & Karger-Kocsis, 2009).

In another work, the effects of CNF and PU into POM on the DMA data are shown in Figure 10 (Siengchin et al., 2010). One can notice that the stiffness values of the POM/CNF composite were slightly higher than that of the neat POM in the whole temperature range. This indicates the reinforcing effect of CNF. As expected, adding PU rubber was associated with a drop in the storage modulus of the POM/PU blend compared to the neat POM. The storage modulus vs. temperature curves of the POM/PU and POM/PU/CNF systems were practically the same. The plots in Figure 10b reveal three relaxation transitions in POM. The glass transition temperature (T_g) is located at around -60 °C (γ-relaxation transition). Another two peaks, observed at ca. -2 °C and ca. 130 °C correspond to the β- and α-relaxations, respectively. These relaxation processes are assigned to the motions of long molecular segments in disordered (β) and well ordered crystalline phases (α), respectively (Hojfors et al., 1977). Incorporation of PU yielded an additional maximum peak at ca. -50 °C in the tan δ vs. T trace, which represents the T_g of the PU component. Adding CNF and/or PU was accompanied with a shift in both the α- and β-relaxations to lower temperatures (ca. 5 °C). One possible explanation is that small agglomerates of CNF and matrix voids within this network support the movement of macromolecular chains yielding a small reduction in the T_g (β-relaxation) of the matrix (Shen et al., 2007).

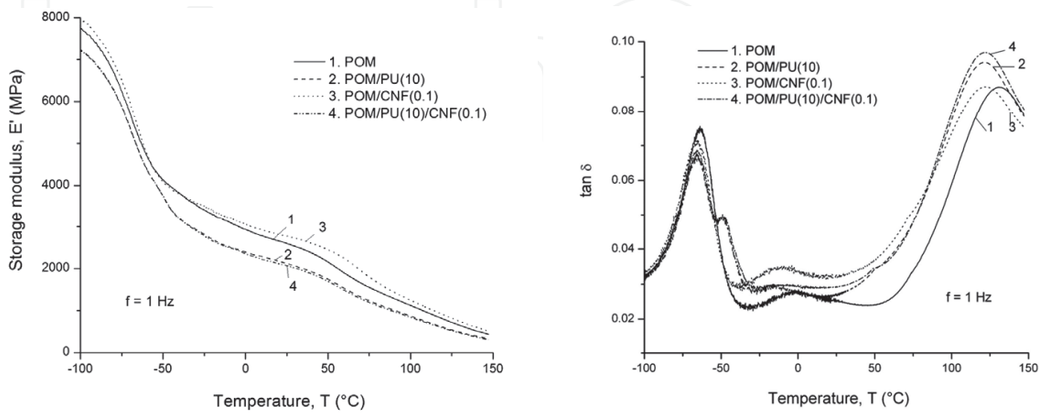

Fig. 10. (a) Storage modulus (E′) and (b) mechanical loss factor tan (δ) as a function of temperature for CNF based on POM composites (Siengchin et al., 2010).

4.1.3 Tensile test

The main advantage of reinforcing thermoplastic composites is the enhancement in the mechanical properties of the thermoplastic matrix at relatively low inorganic filler content. To monitor the reinforcing ability of nanofillers in the thermoplastics matrix of the compound, tensile mechanical test appears as an excellent tool. The effects of CNF and PU on the tensile mechanical data are shown in Figure 11. The enhancement in tensile strength of nanocomposites containing 0.1 wt. % CNF was ca. 18 % compared to the neat POM. The primary reason for that is that due to the uniform dispersion of CNF in POM, an efficient load transfer occurs from the matrix towards the CNF. SEM picture also confirms that the CNF is well dispersed in POM matrix (cf. Figure 5). A fine CNF dispersion is expected already based on the low concentration of CNF in the aqueous suspension used. SEM pictures taken from the fracture surfaces of the specimens indicated that the residual mean length of CNF is ca. 6 μm. Note that a reinforcing effect is generally accompanied with reduced ductility in all composite materials. This is the case also for the POM/CNF nanocomposite the elongation at break value of which is below that of the neat POM. Introducing PU has an adverse effect: the tensile strength decreases, whereas the elongation at break increases markedly. Note that this is the usual response of thermoplastics with impact modifier under static loading conditions. Additional incorporation of CNF increases the tensile strength and reduces the elongation at break of the POM/PU blend confirming that CNF acts as reinforcement.

For the incorporation of FH and BA particles based on HNBR/PA-6 systems (Siengchin & Karger-Kocsis, 2011), the ductility was strongly reduced compared to the PA-6 matrix. Due to the rubbery character of the incorporated HNBR, the PA-6/HNBR blend exhibits markedly lower stiffness than the parent PA-6. However, the elongation at break increases markedly by adding HNBR to PA-6. It is usually accepted that rubber domains first cavitate provoking locally a plane strain/plane stress transition in fracture mechanical terms (Paul & Bucknall, 2000). This supports the development of crazing (with further elongation of the craze fibrils) and superimposed shear yielding, which all enhance the ductility. As expected, the nanoparticle reinforcement leads to increased stiffness and reduced ductility (Siengchin & Karger-Kocsis, 2009; Karger-Kocsis, 2009). The latter is mainly due the stress concentration effects of filler agglomerates which cannot be released by matrix-related events (crazing, shear deformation) owing to inhomogeneous filler dispersion. Stress concentration induces filler/matrix debonding, and the related voids coalescence causing final, premature fracture. The nanocomposite containing FH exhibits higher E-modulus than the companion composite containing BA, though the related value remains under that of the neat PA-6. This relative stiffness increment should be traced to the difference in the dispersion characteristics of FH and BA. Recall that FH was intercalated and mostly dispersed in the PA-6 matrix by contrast to BA being located in the HNBR phase.

To order to investigate the effect of PU and alumina in POM systems,the tensile mechanical data in form of tensile strength, modulus and elongation at break were also studied. Addition of PU to POM or the combined use of PU and alumina improves the elongation at break, however, at cost of the tensile strength. The POM/PU/alumina ternary composites prepared by the masterbatch (MB) method exhibited higher tensile strength accompanied by much higher elongation at break when compared with the composite produced by direct melt compounding (DM) or to the POM/PU blend. Recall that the alumina particles are by far better dispersed in the matrix when prepared via the MB instead of the DM technique. This is in line with recent reports claiming that the tensile mechanical response is strongly

affected by the dispersion state of nanofillers in polystyrene (PS) (Siengchin & Karger-Kocsis, 2006). Moreover, it is worth noting that increased ductility (elongation at break) generally manifests in improved toughness.

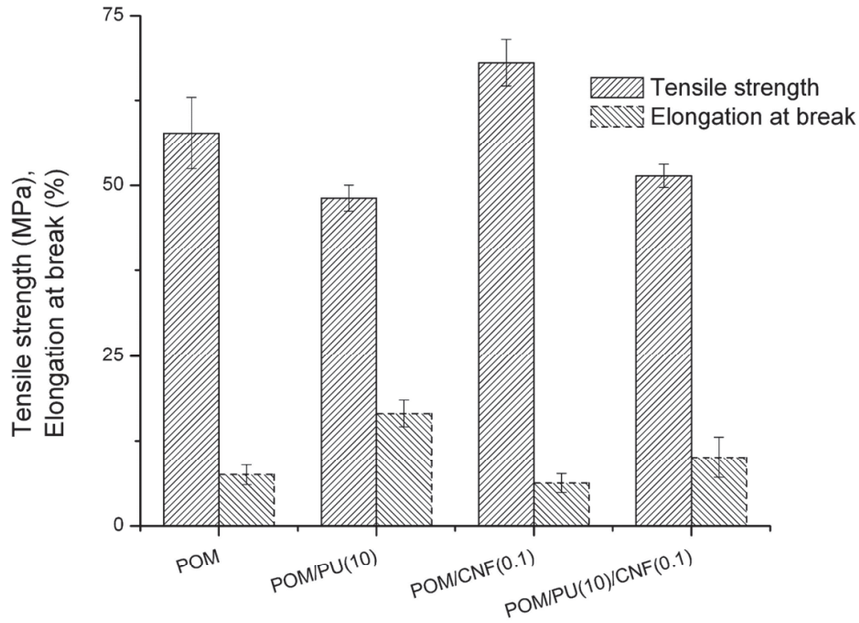

Fig. 11. Tensile strength and elongation at break for CNF based on POM composites (Siengchin et al., 2010).

4.1.4 Dielectric response

Dielectric spectroscopy is a powerful experimental tool for the investigation of polarization and conductivity mechanisms, molecular mobility, phase changes and interfacial phenomena in polymers and polymer matrix composites. Experimental data can be analyzed by means of different formalisms, such as dielectric permittivity, ac conductivity and electric modulus formalism. Although the recorded electrical effects can be described and analyzed in terms of any of the aforementioned formalisms, under certain conditions a specific formalism could be proved more helpful in extracting information with respect to the occurring physical processes. Figure 12 presents the dependence of the dielectric permittivity (ε') and dissipation factor (tan δ) on the frequency, measured at room temperature for all the examined specimens. The dielectric permittivity and dissipation factor attain high values at the low frequency edge, which are decreasing steeply with increasing frequency. Considering the insulating nature of the examined systems, the enhanced values in the low frequency range indicate the co-existence of electrode polarization and interfacial relaxation phenomena. Electrode polarization is an undesirable effect related to the charged electrode-specimen contacts. Interfacial polarization (IP) or Maxwell-Wagner-Sillars (MWS) effects are present in heterogeneous systems because of the accumulation of mobile charges at the interfaces of the composite (Tsangaris & Psarras,

1999). Separating the contribution of each effect is not an easy procedure in the dielectric permittivity mode and thus the electric modulus formalism will be employed for the interpretation of dielectric data.

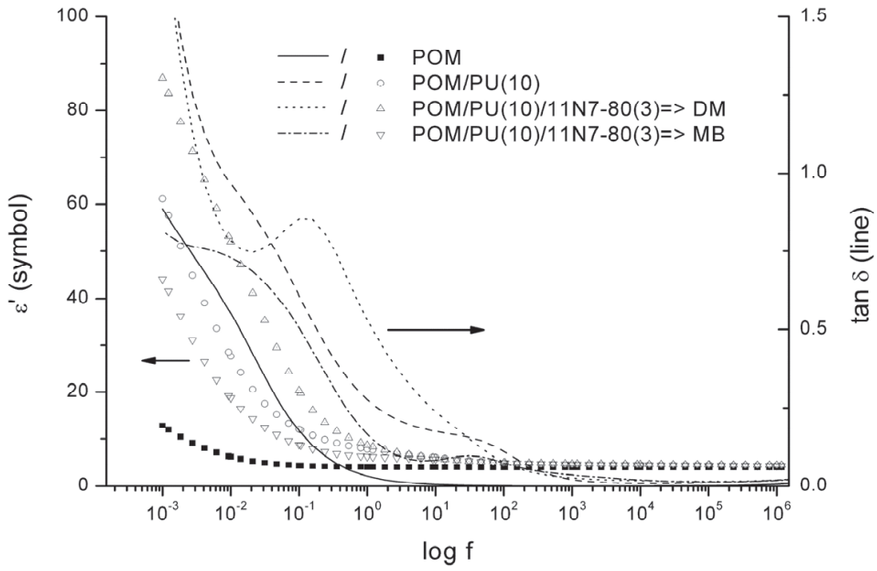

Fig. 12. Dielectric permittivity ($\varepsilon^{'}$) and dissipation factor (tan δ) as a function of frequency (f) for the composites produced by masterbatch (MB) and direct melt compounding (DM) (Siengchin et al., 2008).

Electric modulus presentation exhibits some advantages in the interpretation of slow relaxation phenomena (processes with relatively enhanced relaxation time) in complex systems, mainly because of the elimination of the undesirable effect of electrode polarization (Tsangaris et al., 1998; Psarras et al., 2007).
Electric modulus is defined as the inverse quantity of complex permittivity by the following equation:

$$M^{*} = \frac{1}{\varepsilon^{*}} = \frac{1}{\varepsilon^{'} - j\varepsilon^{''}} = \frac{\varepsilon^{'}}{\varepsilon^{'2} + \varepsilon^{''2}} + j\frac{\varepsilon^{''}}{\varepsilon^{'2} + \varepsilon^{''2}} = M^{'} + jM^{''} \tag{11}$$

where ε' , M′ and ε'' , M″ are the real the imaginary part of dielectric permittivity and electric modulus respectively.
Figure 13a depicts the real part of electric modulus (M′) as a function of frequency for POM, POM/PU blend and the POM/CNF binary- and POM/PU/CNF ternary composites (Siengchin et al., 2010). The real part of electric modulus (M′) as a function of frequency undergoes a step-like transition from low to high values for POM and POM/CNF binary composite. On other hand the POM/PU blend and the POM/PU/CNF ternary composite exhibit, at least, two step-like transitions. These transitions correspond to relaxation processes, which become evident in the loss modulus index vs. frequency plots.

Figure 13b depicts the dielectric spectra of the imaginary part of electric modulus (M'') as a function of the frequency of the applied field. In the case of pure POM a single loss peak is recorded in the low frequency region, which is assigned as α-relaxation. However, at room temperature, and in the examined frequency range only the slower transition is recorded. The origin of this process cannot be ascribed undisputedly. It has been attributed to rearrangements in the crystalline parts of POM, although contributions from the amorphous phase cannot be excluded (Siengchin et al., 2008; Psarras et al., 2007). Since this is the slower occurring relaxation process in POM, it is reasonable to suggest that is related to interfacial polarization phenomena between crystalline and amorphous phases. Interfacial polarization (IP) occurs in heterogeneous and complex systems because of the accumulation of unbounded charges at the interfaces of the phases. The corresponding peak of POM/CNF (0.1) system is not recorded in the examined frequency range, and it seems that is shifted to lower frequencies (cf. Figure 13b). This is a typical behavior for composite systems, where the presence of the reinforcing phase enhances heterogeneity, interfacial polarization and the relative relaxation time (Tsangaris & Psarras, 1999). The situation differs in the case of POM/PU (10) blend and the ternary system POM/PU(10)/CNF(0.1). In their dielectric spectra two relaxation processes are recorded in the intermediate frequency region, while the tendency for the formation of a third peak is present in the high frequency edge. From previous studies (Siengchin et al., 2008; Psarras et al., 2007) it is known that PU, at ambient, has a peak in the vicinity of 100Hz, related to its glass to rubber transition, and tends to form a second one at high frequencies. The latter is attributed to reorientation of polar side groups of the main chain (Psarras et al., 2007). Systems containing PU exhibit the aforementioned loss peaks. However, the third peak (the slower process) recorded close to 0.1Hz cannot be connected with PU, and thus it should be assigned to POM. The peak locus of POM's α-mode appears to shift to higher frequencies by almost an order of magnitude in the POM/PU(10) and POM/PU(10)/CNF(0.1) systems, indicating that the processes became faster.

The dielectric response of the examined systems is influenced by their variations in morphology. As it is already stated the presence of PU affects the morphology of POM by disturbing the spherulitic structure of the latter. The extent of rigid crystalline regions is diminishing, rearrangement of crystallites and/or relaxation of isolated amorphous segments is facilitated and thus the peak of α-mode shifts to higher frequencies. Moreover the incorporation of CNF reduces further the size of spherulites (cf. Figure 14) and consequently increases the interfacial area between the constituents and phases of the nanocomposite. The presence of CNF in the ternary system slightly influences the position of the peak by shifting to lower frequency, and at the same time reduces the intensity of electric modulus loss index (M''). In the dielectric permittivity formalism, enhanced heterogeneity and extensive interfacial area yield to increased values of the real and imaginary part of permittivity (ε') and (ε'') respectively, at low frequencies. Recalling electric modulus equation, it should be noted that the same data expressed in the electric modulus formalism would provide reducing values of the real and imaginary part of electric modulus (M') and (M'') respectively, with the increase of heterogeneity and interfacial area. Under this point of view, it is reasonable to suggest that the specific relaxation mode, recorded in the vicinity of 0.1Hz, is influenced by interfacial polarization phenomena, which are strengthen in the case of the ternary system.

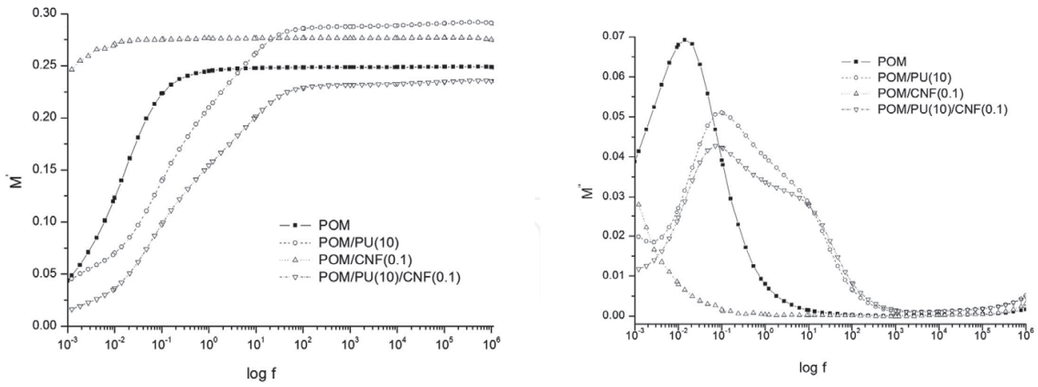

Fig. 13. (a) real (M′) and (b) imaginary part (M′′) versus frequency traces for CNF based on POM composites (Siengchin et al., 2010).

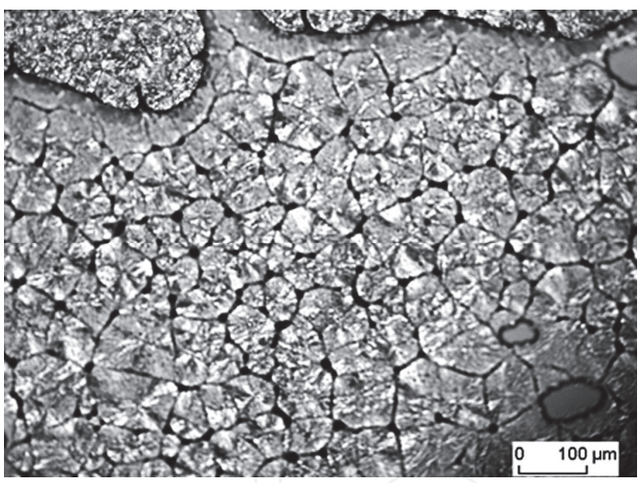

Fig. 14. Polarized light microscopy image for POM/PU/CNF ternary composite (Siengchin et al., 2010).

4.1.5 Stress relaxation

In order to describe the stress relaxation results phenomenological models, composed of spring and dashpot elements, are frequently used. Their parameters do not depend on the level of the applied deformation in the linear viscoelastic range according to the theory of viscoelasticity. For stress relaxation under applied constant strain (ε_0) the material response is given by:

$$E_r(t) = \frac{\sigma(t)}{\varepsilon_0} \tag{12}$$

where $E_r(t)$ is the stress relaxation modulus, and $\sigma(t)$ is stress, both as a function of time (t).

In the nonlinear range the dependence upon the level of the applied deformation can be expressed by multiplying the linear parameters by so-called nonlinearity factors, which are deformation-, time- and temperature-dependent. The nonlinear stress relaxation modulus is given by:

$$E_r\left(t,\varepsilon(t),T\right)=\frac{\sigma\left(t,\varepsilon(t),T\right)}{\varepsilon_0} \tag{13}$$

where $\varepsilon(t)$ is the real strain at time (t) and T is the temperature.
The stress relaxation data, measured in function of time for the POM, POM/PU blend and the CNF-containing binary-, and ternary composites is shown in Figure 15. The shape of the relaxation curves of the systems is similar to that of the neat POM. However, their relaxation modulus decreased remarkably with incorporation of PU compared to the neat POM. One can see that the relaxation modulus of the POM/CNF binary composite is slightly higher in the whole relaxation time range than those of the POM, POM/PU blend and POM/PU/CNF ternary composite. The increase of the relaxation modulus with CNF content is due to its reinforcing effects. Note that the long CNFs may relieve very efficiently such stress concentration effects which are induced by material heterogeneities. This finding is coherent with those deduced from creep (cf. Figures 4), DMA (cf. Figure 10) and tensile mechanical tests (cf. Figure 11).

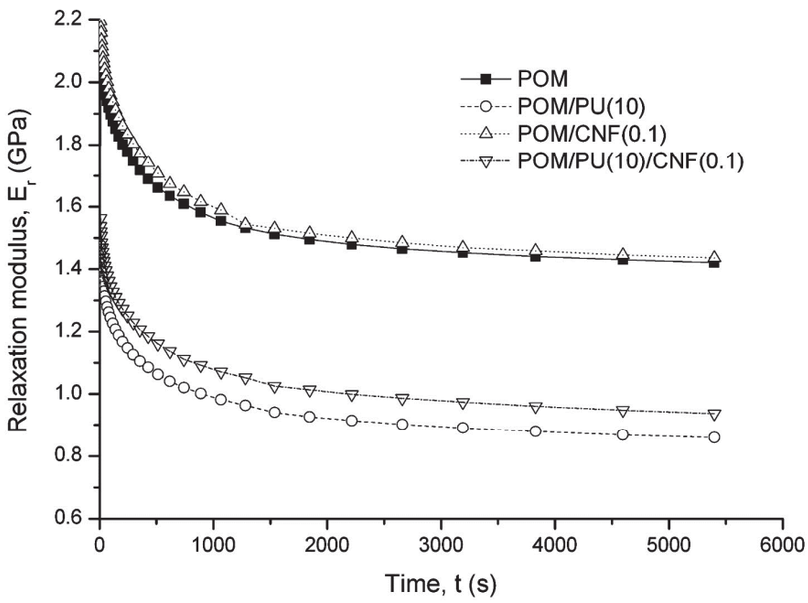

Fig. 15. Relaxation modulus for CNF based on POM composites (Siengchin et al., 2010).

4.1.6 Thermo-oxidative properties

It has been reported that by adding inorganic fillers (Sun et al., 2007), may increase the thermal stability of thermoplastics. This is at odds with our TGA observation. Figure 16 shows the weight loss vs. temperature traces for the POM, POM/PU blend, POM/CNF binary, and POM/PU/CNF ternary composites (Siengchin et al., 2010). The thermal degradation of the neat POM is a one-step procedure representing depolymerization. Incorporation of PU reduces slightly, whereas CNF markedly the onset of the thermal degradation. The follow-up degradation of the POM/CNF runs, however, at higher temperature than both POM and POM/PU blend. The POM/PU/CNF ternary composite has the highest onset decomposition temperature. Moreover, the related mass loss vs. temperature trace is parallel shifted to that of the POM towards higher temperatures. The common use of PU and CNF resulted in a synergistic effect in the thermo-oxidative stability of POM.

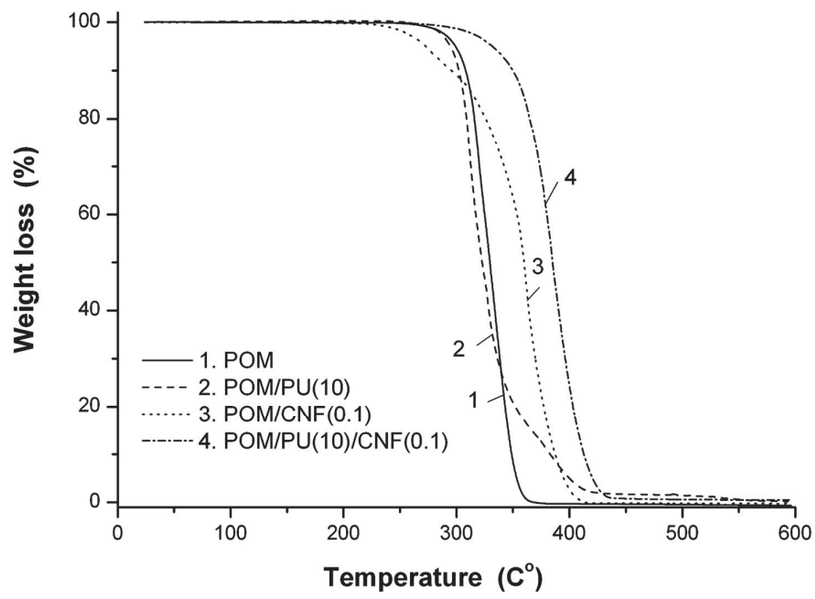

Fig. 16. Weight loss versus temperature for CNF based on POM composites (Siengchin et al., 2010).

4.2 Nanocomposites produced by WMC

Latex melt compounding techniques to disperse various rubber and nanofillers was already tried for various thermoplastic systems. This part of book chapter addresses the toughening and reinforcement of polyoxymethylene (POM) via a water-assisted melt compounding technique (above process) which is allow us to produce nanocomposites with additional

toughening. Polyurethane (PU) was selected as toughening agent for POM according to the state-of-art. It was used in its latex form. It is noteworthy that the mean size of rubber latices is closely matched with that of conventional toughening agents, impact modifiers. Synthetic boehmite alumina was used as nanofiller. One of the criteria for selecting this filler was that it is water dispersible and thus its nanoscale dispersion can be achieved also in aqueous polymer latex.

Toughened or nanofilled POM composites have been successfully produced by water-assisted melt compounding technique. TEM results have shown that the alumina and rubber dispersions became fine and homogeneous when using the water-assisted extrusion melt compounding. The alumina particles are nanoscaled and homogeneously dispersed in the matrix (cf. Figure 17a). Figure 17b demonstrates that the PU rubber particles are also well dispersed in the POM matrix. The mean diameter of the PU is 700-900 nm, which is closely matched with the initial size of the PU particles in the corresponding latex. In the POM/PU/alumina ternary composites the alumina particles are mainly in the PU phase. On the other hand, the alumina and rubber particles are also separately dispersed in the POM matrix.

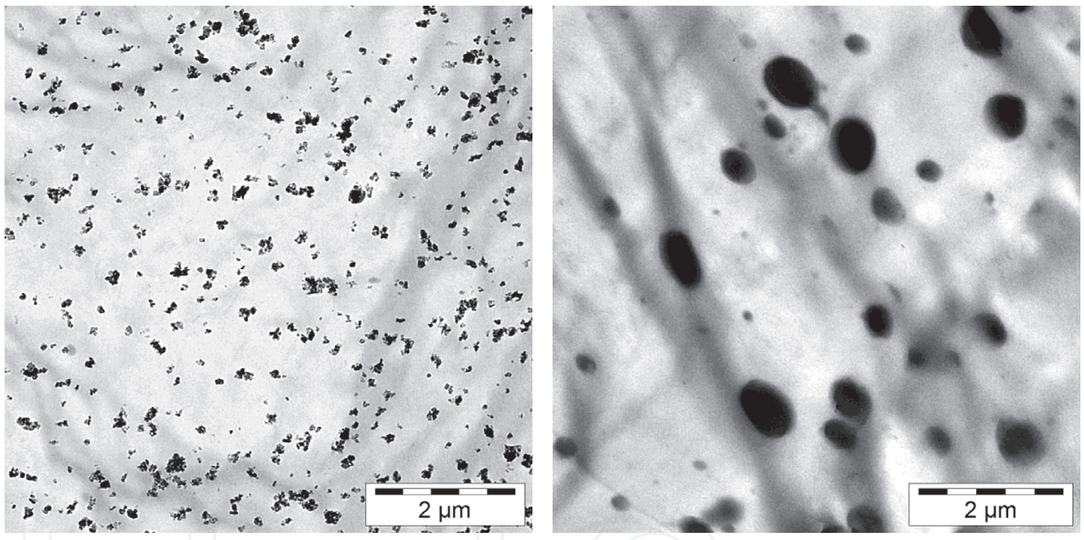

Fig. 17. TEM images of (a) POM/alumina composite and (b) POM/PU blend.

Reinforcement is defined as the ability of nanofillers to improve a variety of thermoplastic properties, e.g. tensile strength and stiffness. The reinforcement effect can be explained using DMA and creep diagrams. The tensile storage- and tan δ curve of nanoreinforced thermoplastic composites is shows up to a higher stiffness compared to an unfilled matrix. From this observation a reinforcing effect can be seen in Figure 18 (Siengchin et al., 2008). The modulus E' of POM systems decreases with increasing temperature and the stiffness of the POM/PU blend was lower than the POM. However, the incorporation of alumina particles resulted in some increase in the storage modulus in the whole temperature range, compared to that of the pure POM. This can be well explained by reinforcing effect of alumina particles leading to an increased stiffness. In addition, the blend containing 10 wt% of PU exhibits markedly higher loss modulus than the other systems. This is due to the rubbery character of the incorporated PU.

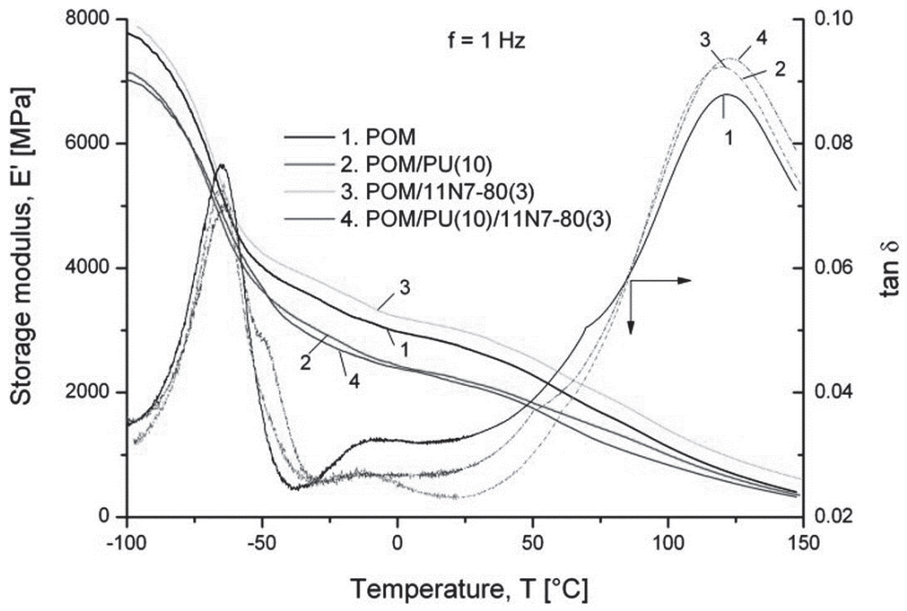

Fig. 18. Storage modulus (E′) and mechanical loss factor tan (δ) as a function of temperature for the composites produced by water-assisted extrusion melt compounding (Siengchin et al., 2008).

Generally, the creep behaviour of material is predicted by Burgers model (Findley et al., 1989). This creep model proved to be successfully applicable for many polymers. Therefore, this model is used to evaluate the effect of rubber particles and fillers in composites prepared by water-assisted melt compounding method. The creep experiment can be calculated from a discrete retardation spectrum of the Burgers model consisting of a Maxwell and a Kevin units connected in series by the equation (Kaschta & Schwarzl, 1994):

$$D(t)=D_0+\Psi(t)+\frac{t}{\mu_0} \tag{14}$$

$$\Psi(t)=\sum_{k=1}^{N} D_k * \left[1-e^{-t/\tau_k}\right] \tag{15}$$

where t is the time, D_0 is the instantaneous compliance, $\Psi(t)$ is equilibrium compliance part of creep compliance, μ_0 is viscosity and τ is different retardation times of the Kelvin unit D_k.

Figure 19 displays the traces of the creep compliance and its simulated value using the Burgers model, as a function of time at T=30 °C for the POM, POM/alumina composite, POM/PU blend and the alumina-containing ternary composites produced by water-assisted melt compounding. The incorporation of alumina particles into POM matrix resulted in a considerable decrease of the creep compliance, as expected owing to their reinforcing effect. Conversely, the addition of PU increased the creep of POM. The compliance values were

reduced by approx. 12 % compared to the POM/PU blend when alumina was additionally incorporated. This creep response suggests that alumina and rubber particles are fine dispersed in the POM matrix. This was supported by the SEM inspection (cf. Figure 17). This phenomenological Burgers model was used to evaluate the effect of rubber and/or alumina particles on the instantaneous and equilibrium parts (approximated by six Voigt-Kelvin elements) of the creep compliance. The highest instantaneous compliance (D_0) was observed when PU was added into the POM. The instantaneous compliance of the POM/alumina composite is lower than those of the POM and POM/PU blend. The enhancement in the instantaneous part of compliance is caused by the alumina particles and their dispersed state. This resulted in a decrease in the mobility of the amorphous segments.

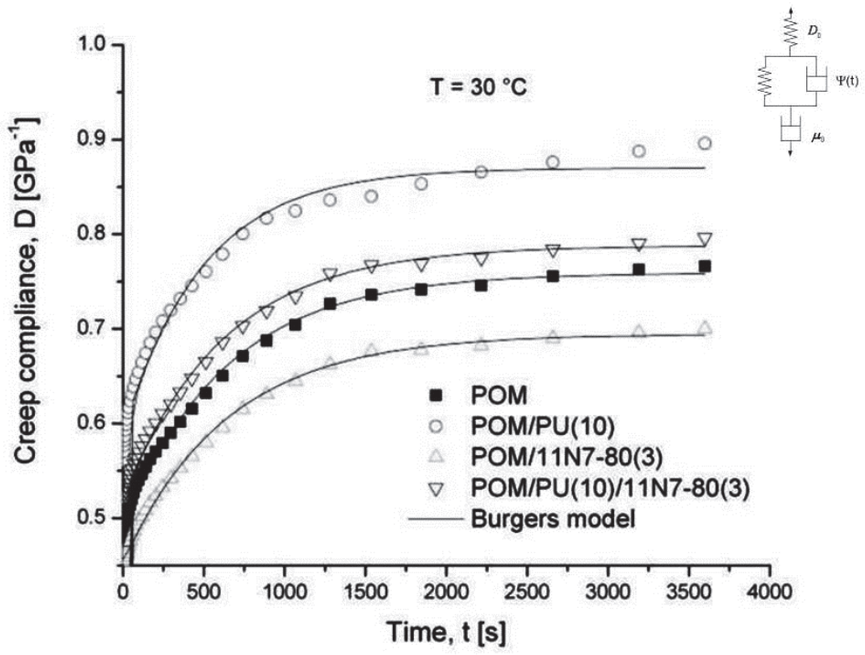

Fig. 19. Creep compliance for the composites produced by water-assisted extrusion melt compounding, fitted by Burgers model (Siengchin et al., 2008).

Results of the tensile mechanical tests of composites prepared by WMC are given in Table 1 model (Siengchin et al., 2008). It is clear by seen that the incorporation of alumina and PU particles strongly affected the mechanical behavior of POM. Adding alumina increased the stiffness slightly reduced the strength, the elongation at break. Conversely, the ductility of the POM/PU blend increased and the stiffness and strength decreased compared to pure POM. The reduction in the tensile strength may be attributed to the presence of rubber particles acting as stress concentrators and forcing the yielding at lower stresses. The decrease in the tensile modulus in the POM/PU blend may be accounted for the softening effect of PU, since the tensile modulus of rubber is considerably lower than that of the pure POM. The POM/PU/alumina ternary composites exhibited significant decrease in modulus accompanied by much higher elongation at break as compared to the POM, POM/alumina composite and POM/PU blend.

Sample Designation	Tensile strength [MPa]	Tensile modulus [MPa]	Elongation at break [%]
POM	63± 0.2	2646±71	17.8±2.8
POM/PU(10)	55± 0.2	2392±101	31.9±4.5
POM/alumina	61± 0.1	2847±143	9.1±2.8
POM/PU(10)/alumina	47± 0.5	2323±62	57.1±8

Table 1. Tensile mechanical characteristics of the composites produced by water-assisted extrusion melt compounding model (Siengchin et al., 2008).

Toughness is the ability of a material to absorb energy. The toughness can be done by using a pendulum and basic physics to measure how much energy it will be hold. Figure 20 shows the impact energy of POM, POM/PU blend and the composites with alumina particles produced by WM-CT model (Siengchin et al., 2008). Even though the tensile modulus of POM is increased by the incorporation of rigid alumina particles, the toughness was reduced. However, POM modified with 10 wt.% PU exhibit not only higher elongation at break, but similarly also higher impact energy (ca. 22 %) compared to the pure POM. This is due to the submicron dispersion of the rubber particles. So, the incorporation of rubbery particles in a suitable size range increases the impact resistance of POM. Furthermore, the impact energy of POM/PU/alumina ternary composites was marginally decreased compared to the POM/PU blend but remained still higher than POM.

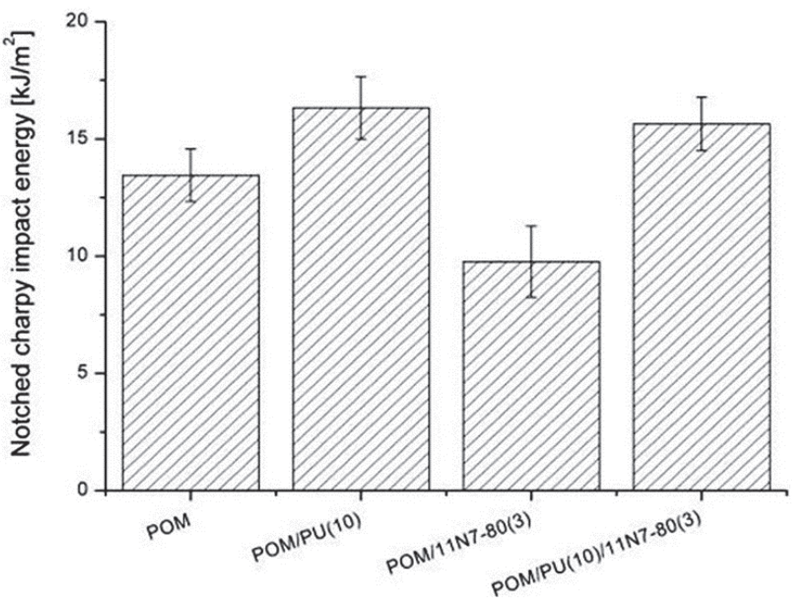

Fig. 20. the impact energy for the composites produced by water-assisted extrusion melt compounding model (Siengchin et al., 2008).

5. Summary

This chapter was devoted to develop the melt-compounding methods to manufacture tough, nanofiller-reinforced thermoplastics by adding an aqueous filler slurry and/or rubber dispersion to the molten polymer followed by evaporation of the water carrier. The

work also compared the morphological, mechanical and thermal properties of nanoreinforced/toughened thermoplastic composites produced by latex melt compounding (LMC) and water-assisted melt compounding (WMC). Toughened or reinforced thermoplastic composites have been successfully produced by WMC. The mechanical properties (stiffness and creep resistance) of the composites were superior to those of the POM and POM/PU blend. The impact resistance of POM was highly enhanced by the addition of PU rubber. The dispersed rubber particle size was closely matched with that one required from usual toughening agents, impact modifiers. Besides, this WMC is a very effective process being simple and cost efficient for producing composite materials, as the expensive chemical modification of the nanofillers can be avoided. The water-assisted melt compounding to produce nanocomposites containing fillers- and rubber particles as nanoscale reinforcements and toughness offers a general way to modify the properties, such as stiffness and toughness. However, the toughened properties of and reinforced nanocomposites should be optimized via various rubber/filler ratios and concentrations.

Greek Symbols

$\varepsilon, \varepsilon_0$	Strain-, amplitude of the strain
$\varepsilon', \varepsilon''$	Real-, imaginary permittivity
ψ	Equilibrium compliance part
σ	Stress
σ_0	Applied constant stress
ω	Angular frequency
μ_0	Viscosity (Strain)
τ	Retardation time
δ	Phase angle shift

6. Acknowledgement

I am grateful to King Mongkut's University of Technology North Bangkok for providing me the opportunity of working in an outstanding environment from the scientific and technical point of view. Especially I would like to express my special thanks to Ms. Pawinee Boonyasopon who constantly support and encourage me.

7. References

Borggreve, R.J.M., Gaymans, R.J. & Schuijer, J. (1987). Impact behaviour of nylon-rubber blends: 5. Influence of the mechanical properties of the elastomer. *Polymer,* Vol. 30, No.1, pp. 71-77, ISSN 0032-3861

Margolina, A. & Wu, S. (1988). Percolation model for brittle-tough transition in nylon/rubber blends. *Polymer,* Vol. 29, No. 12, pp. 2170-2173, ISSN 0032-3861

Baldi, F., Bignotti, F., Tieghi, G. & Riccò T. (2006). Rubber toughening of polyamide 6/organoclay nanocomposites obtained by melt blending. *Journal of Applied Polymer Science*, Vol. 99, No. 6, pp. 3406-3416, ISSN 0021-8995

Wu, S. (1988). A generalized criterion for rubber toughening: The critical matrix ligament thickness. *Journal of Applied Polymer Science,* Vol. 35, No. 2, pp. 549-561, ISSN 0021-8995

Jiang, W., Yuan, Q., An, L. & Jiang, B. (2002). Effect of cavitations on brittle-ductile transition of particle toughened thermoplastic. *Polymer Communication,* Vol. 43, No. 4, pp. 1555-1558, ISSN 0032-3861

Kumar, S., Doshi, H., Srinivasarao, M., Park, J.O. & Schiraldi, D.A. (2002). Fibers from polypropylene/nano carbon fiber composites. *Polymer,* Vol. 43, No.5, pp. 1701-1703, ISSN 0032-3861

Chung D.D.L. (2001). Comparison of submicron-diameter carbon filaments and conventional carbon fibers as fillers in composite materials. *Carbon,* Vol. 39, No. 8, pp. 1119-1125, ISSN 0008-6223

Sandler, J. Werner, P., Shaffer, M.S.P., Demchuk, V., Altstaedt, V. & Windle, A.H. (2002). Carbon nanofibre reinforced poly(ether ether ketone) composites. *Composites Part A,* Vol. 33, No. 8, pp. 1033-1039, ISSN 1359-835x

Puglia, D., Valentine, L. & Kenny, J.M. (2003). Analysis of the cure reaction of carbon nanotubes/epoxy resin composites through thermal analysis and Raman spectroscopy. *Journal of Applied Polymer Science*, Vol. 88, No. 2, pp. 452-458, ISSN 0021-8995

Song, Y.S. & Youn, J.R. (2005). Influence of dispersion states of carbon nanotubes on physical properties of epoxy nanocomposites. *Carbon,* Vol. 43, No. 7, pp. 1378-1385, ISSN 0008-6223

Kinloch, I.A., Roberts, S.A. & Windle, A.H. (2002). A rheological study of concentrated aqueous nanotube dispersions. *Polymer,* Vol. 43, No. 26, pp. 7483-7491, ISSN 0032-3861

Gryschuck, O., Karger-Kocsis, J., Thomann, R., Kanya, Z. & Kiricsi, I. (2006). Multiwall carbon nanotube modified vinylester and vinylester – based hybrid resins. *Composites Part A,* Vol. 37, No. 9, pp. 1252-1259, ISSN 1359-835x

Ruan, S.L., Gao, P., Yang, X.G. & Yu, T.X. (2003). Toughening high performance unltrahigh molecular weight polyethylene using multiwalled carbon nanotubes. *Polymer,* Vol. 44, No.19, pp. 5643-5654, ISSN 0032-3861

Lozano, K., Yang, S. & Jones, R.E. (2004). Nanofiber toughened polyethylene composites. *Carbon,* Vol. 42, No. 11, pp. 2329-2331, ISSN 0008-6223

Seyhan A.T., Sun, Z., Deitzel. J., Tanoglu, M. & Heider, D. (2009). Cure kinetics of vapor grown carbon nanofiber (VGCNF) modified epoxy resin suspensions and fracture toughness of their resulting nanocomposites. *Materials Chemistry and Physics*. Vol. 118, No. 1, pp. 234-242, ISSN 0254-0584

Sui, G., Jana, S., Zhong, W.H., Fuqua, M.A. & Ulven, C.A. (2008). Dielectric properties and conductivity of carbon nanofiber/semi-crystalline polymer composites. Acta Materialia, Vol. 56. No. 10, pp. 2381-2388, ISSN 1359-6454

Sui, G., Zhong, W.H., Ren, X., Wang, X.Q. & Yang, X.P. (2009). Structure, mechanical properties and friction behavior of UHMWPE/HDPE/carbon nanofibers. *Materials Chemistry and Physics*. Vol. 115, No. 1, pp. 404-412, ISSN 0254-0584

Prolongo, S.G., Campo, M., Gude, M.R., Chaos-Morán, R. & Ureña, A. (2009). Thermo-physical characterisation of epoxy resin reinforced by amino-functionalized carbon nanofibers. *Composites Science and Technology*, Vol. 69, No. 3-4. pp. 349-357, ISSN 0266-3538

Lozano, K., Files, B., Rodriguez-Macias, F. & Barrera, E.V. (1999). Purification and functionalization of vapor grown carbon fibers and single wall nanotubes.

Symposium Powder Materials: Current Research and Industrial Practices (Cincinnati OH, USA), *TMS fall meeting*, pp. 333-340

Park, E.J., Heo, H. & Lim, K. T. (2007). Synthesis and characterization of $Al(OH)_3$/ polystyrene nanocomposite latex particles by emulsion polymerization. *Macromolecular Symposia*, Vol. 249-250, No. 1, pp. 247-250, ISSN 1521-3900

Akelah, A. & Moet, A. (1996). Polymer-clay nanocomposites: free-radical grafting of polystyrene on to organophilic montmorillonite interlayers. *Journal of Materials Science,* Vol. 31, No. 13, pp. 3589-3596, ISSN 0022-2461

Wang, D., Zhu, J., Yao, Q. & Wilkie, C.A. (2002). A comparison of various methods for the preparation of polystyrene and poly(methylmethacrylate) clay nanocomposites. *Chemistry of Materials,* Vol. 14, No. 9, pp. 3837-3843, ISSN 0897-4756

Chen, G., Qi, Z. & Shen, D. (2000). Shear-induced ordered structure in polystyrene/clay nanocomposite. *Journal of Materials Research,* Vol. 15, No. 2, pp. 351-356, ISSN 0884-2914

Zhou, Q., Fan, X., Xia, C., Mays, J. & Advincula, R. (2001). Living anionic surface initiated polymerization (SIP) of styrene from clay surfaces. *Chemistry of Materials,* Vol. 13, No. 8, pp. 2465-2467, ISSN 0897-4756

Jana, S.C. & Jain, S. (2001). Dispersion of nanofillers in high performance polymers using reactive solvents as processing aids, *Polymer,* Vol. 42, No. 16, pp. 6897–6905, ISSN 0032-3861

Siengchin, S., Karger-Kocsis, J., Apostolov, A.A. & Thomann, R. (2007). Polystyrene-fluorohectorite nanocomposites prepared by melt mixing with latex precompounding: Structure and mechanical properties, *Journal of Applied Polymer Science*, Vol. 106, No. 1, pp. 248-254, ISSN 0021-8995

Grunlan, J.C., Mehrabi, A.R. & Bannon, M.V. (2004). Water-based single-walled-nanotube-filled polymer composite with an exceptionally low percolation thershold. *Advanced Materials,* Vol. 16, No. 2, pp. 150-153, ISSN 0935-9648

Xia, H., song, M., Zhang, Z. & Richardson, M. (2007). Microphase separation, stress relaxation, and creep behavior of polyurethane nanocomposites. *Journal of Applied Polymer Science,* Vol. 103, No. 5, pp. 2992-3002, ISSN 0021-8995

Eckstein, A., Suhm, J., Friedrich, C., Maier, R.D., Sassmannshausen, J., Bochmann, M. & Mülhaupt, R. (1998). Determination of plateau moduli and entanglement molecular weights of isotatic, sydiotactic, and atactic polypropylenes synthesized with metallocene catalysts. *Macromolecules,* Vol. 31, No. 4, pp. 1335-1340, ISSN 0024-9297

Schapery, R.A. (1969). On the characterization of nonlinear viscoelastic materials. *Polymer Engineering and Science,* Vol. 9, No. 4, pp. 295-310, ISSN 0032-3888

Brueller, O.S. (1987). On the nonlinear characterization of the long term behavior of polymeric materials. *Polymer Engineering and Science,* Vol. 27, No. 2, pp. 144-148, ISSN 0032-3888

Siengchin, S., Psarras, G.C. & Karger-Kocsis, J. (2010). POM/PU/carbon nanofiber composites produced by water-mediated melt compounding: structure, thermomechanical and dielectrical properties. *Journal of Applied Polymer Science,* Vol. 117, No. 3, pp. 1804-1812, ISSN 0021-8995

Siengchin, S. & Karger-Kocsis, J. (2009). Structure and creep response of toughened and nanoreinforced polyamides produced via the latex route: Effect of nanofiller type. *Composites Science and Technology*, Vol. 69, No. 5. pp. 677-683, ISSN 0266-3538

Siengchin, S., Karger-Kocsis, J., Psarras, G.C. & Thomann, R. (2008). Polyoxymethylene/polyurethane/alumina ternary composites: structure,

mechanical, thermal and dielectrical properties. *Journal of Applied Polymer Science,* Vol. 110, No. 3, pp. 1613-1623, ISSN 0021-8995

Shaw, M.T. & MacKnight, W.J (2005) Introduction to polymer viscoelasticity, John Wiley & Sons, ISBN 9780471740452, New York

Araújo, E.M., Hage, E. & Carvalho, A.J.F. (2004). Thermal properties of nylon6/ABS polymer blends: Compatibilizer effect. J Materials Science, Vol. 39, No. 4, pp. 1173-1178, ISSN 0022-2461

Hojfors, R.J., Baer, E. & Geil, P.H. (1977). Dynamic-mechanical study of molecular motions in solid polyoxymethylene copolymer from 4 to 315 °K. *Journal of Macromolecular Science, Part B Physics,* Vol. B13, No. 3, pp. 323-348, ISSN: 0022-2348

Shen, J., Huang, W., Wu, L., Hu, Y. & Ye, M. (2007). The reinforcement role of different amino-functionalized multi-walled carbon nanotubes in epoxy nanocomposites. *Composites Science and Technology*, Vol. 67, No. 15-16. pp. 3041, ISSN 0266-3538

Siengchin, S. & Karger-Kocsis, J. (2011). Structure, mechanical and fracture properties of nanoreinforced and HNBR-toughened polyamide-6. *Journal of Applied Polymer Science,* in press, ISSN 0021-8995

Paul, D.R. & Bucknall, C.B. (2000). *Polymer blends: Formulation and Performance,* Vol. 2, John Wiley & Sons, ISBN 0-471-35280-2, New York

Karger-Kocsis, J. (2009). On the toughness of "nanomodified" polymers and their traditional polymer composites, In: *Nano- and Micromechanics of Polymer Blends and Composites,* Chapter 12, Karger-Kocsis, J., Fakirov, S., (Eds.), 425-470, Hanser, ISBN 978-3-446-41323-8, Munich, Germany

Siengchin S. & Karger-Kocsis, J. (2006). Creep behaviour of polystyrene/fluorohectorite micro- and nanocomposites. *Macromolecular Rapid Communications,* Vol. 27, No. 24, pp. 2090-2094, ISSN: 1521-3927

Tsangaris, G. M. & Psarras, G. C. (1999). The dielectric response of a polymeric three-component composite. *Journal of Materials Science,* Vol. 34, No. 9, pp. 2151-2157, ISSN 0022-2461

Tsangaris, G.M., Psarras, G.C. & Kouloumbi, N. (1998). Electric modulus and interfacial polarization in composite polymeric systems. *Journal of Materials Science,* Vol. 33, No. 8, pp. 2027- 2037, ISSN 0022-2461

Psarras, G.C., Gatos, K.G., Karahaliou, P.K., Georga, S.N., Krontiras, C.A. & Karger-Kocsis, J. (2007). Relaxation phenomena in rubber/layered silicate nanocomposites. *Express Polymer letters,* Vol. 1, No. 12, pp. 837-845, ISSN 1788-618X

Psarras, G.C.; Gatos, K.G. & Karger-Kocsis, J. (2007). Dielectric properties of layered silicate-reinforced natural and polyurethane rubber nanocomposites. *Journal of Applied Polymer Science,* Vol. 106, No. 1, pp. 1405-1411, ISSN 0021-8995

Sun, T. J., Ye, L. & Zhao, X. W. (2007). Thermostabilising and nucleating effect of montmorillonite on polyoxymethylene. *Plastics Rubber Composites,* Vol. 36, No. 7-8, pp. 350, ISSN 1465-8011

Siengchin, S., Karger-Kocsis, J. & Thomann, R. (2008). Nanofilled and/or toughened POM composites produced by water-mediated melt compounding: Structure and mechanical properties. *Express Polymer letters,* Vol. 2, No. 10, pp. 746-756, ISSN 1788-618X

Findley, W.N., Lai, J.S. & Onaran, K. (1989). *Creep and relaxation of nonlinear viscoelastic materials,* Dover Publications, ISBN 978-0-486-66016-5, New York, USA

Kaschta, J. & Schwarzl, F. R. (1994). Calculation of discrete retardation spectra from creep data-I. Method. *Rheologica Acta,* Vol. 33, No. 6, pp. 517-529, ISSN 0035-4511

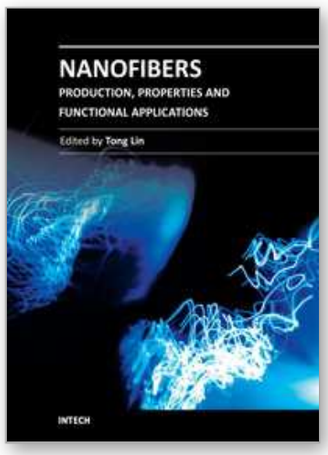

Nanofibers - Production, Properties and Functional Applications
Edited by Dr. Tong Lin

ISBN 978-953-307-420-7
Hard cover, 458 pages
Publisher InTech
Published online 14, November, 2011
Published in print edition November, 2011

As an important one-dimensional nanomaterial, nanofibers have extremely high specific surface area because of their small diameters, and nanofiber membranes are highly porous with excellent pore interconnectivity. These unique characteristics plus the functionalities from the materials themselves impart nanofibers with a number of novel properties for advanced applications. This book is a compilation of contributions made by experts who specialize in nanofibers. It provides an up-to-date coverage of in nanofiber preparation, properties and functional applications. I am deeply appreciative of all the authors and have no doubt that their contribution will be a useful resource for anyone associated with the discipline of nanofibers.

InTech Europe
University Campus STeP Ri
Slavka Krautzeka 83/A
51000 Rijeka, Croatia
Phone: +385 (51) 770 447
Fax: +385 (51) 686 166
www.intechopen.com

InTech China
Unit 405, Office Block, Hotel Equatorial Shanghai
No.65, Yan An Road (West), Shanghai, 200040, China
中国上海市延安西路65号上海国际贵都大饭店办公楼405单元
Phone: +86-21-62489820
Fax: +86-21-62489821

IntechOpen